JOURNAL OF MATERIALS SCIENCE 7 (1972) 631–648

Filamentary Sapphire

Part 1 *Growth and Microstructural Characterisation*

J. T. A. POLLOCK*
Tyco Laboratories, Inc, Bear Hill, Waltham, Massachusetts 02154, USA

An experimental study of the continuous melt growth of filamentary *c*-axis sapphire is presented. The filament had a nominal 0.025 cm diameter and was grown at rates of 2.5 to 7.5 cm/min using the "edge-defined, film-fed growth" technique. Filament growth was recorded and characterised using both single frame photography and 16 mm motion picture photography. Samples were examined after growth using transmitted light metallography. The primary structural characteristic of the material at all growth rates is the presence of 1 μm voids, arranged in patterns which are dependent on both growth rate and temperature. In samples grown at rates up to 6.0 cm/min these voids assume nearly conical arrays which are directly related to the crystallographic rhombohedral planes in sapphire. At 7.5 cm/min the voids outline the edges of cell walls. Based on the hypothesis that they are shrinkage voids and the end result of liquid entrapment behind the advancing solid interface, mechanisms are proposed by which this entrapment might occur at different growth speeds. Using experimental data the stability of the growth process with respect to the constancy of the filament diameter is quantitatively related to both growth rate and temperature.

1. Introduction

Details of a new crystal growth method called "edge-defined, film-fed growth" (EFG) have recently been made available in the literature [1-4]. This novel technique allows the growth of a variety of cross-sectional shapes by making use of a shaped die. The liquid pool from which the crystal is withdrawn is formed on the top surface of the shaped die. The pool is fed by capillaries in the die which extend down into a molten reservoir. The edge-definition, which is the most important part of the method is maintained by the geometry of the top of the die and the fulfilment of a contact angle requirement between the liquid and the die material.

EFG was the outcome of investigations aimed at the production of continuous lengths of sapphire (α-Al_2O_3) filament for use as a structural reinforcement in composite materials. Although the method has been extended to the melt growth of many other materials and cross-sectional shapes, the technique has been most extensively studied through the growth of filamentary sapphire. The purpose of this paper is to present a study of the growth and substructure of *c*-axis ($\langle 0001 \rangle$) sapphire filament grown at rates in the range 2.5 to 7.5 cm/min. This experimental study, which was recorded using both single frame photography and 16 mm motion photography, presents for the first time a visual description of the EFG technique. A second paper will present mechanical data characterising the tensile strength of filament grown under conditions identical with those described in this paper.

2. Experimental

2.1. Crystal Growth Apparatus

The crystal growth apparatus is shown schematically in fig. 1. A carbon susceptor heated by a 450 kc induction unit is used to raise the molybdenum crucible containing the α-Al_2O_3 melt to the growth temperature. An argon atmosphere is maintained within the inner of two concentric quartz tubes between which cooling water flows. The melt and growth area are

*Present Address: AAEC Research Establishment, Materials Division, Lucas Heights, Sutherland 2232, New South Wales, Australia.

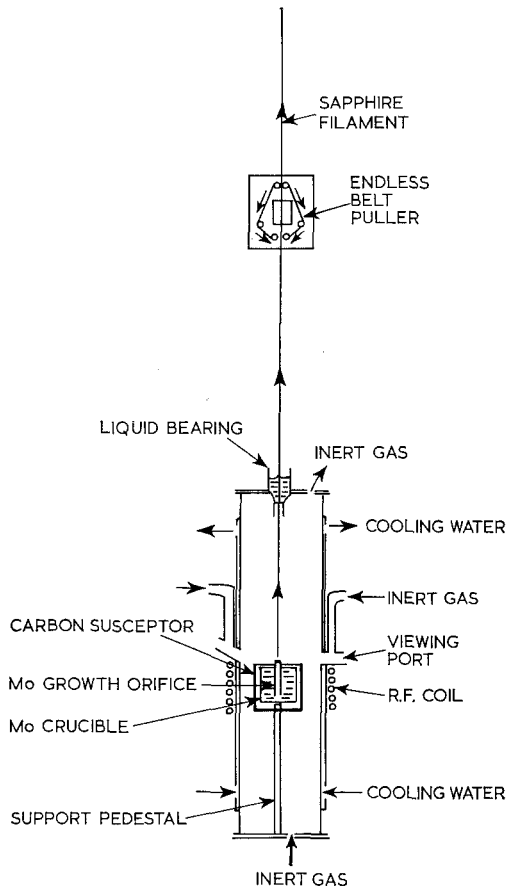

Figure 1 Schematic diagram of crystal growth apparatus.

viewed directly through either of the windowless ports which allow undistorted observation. These ports operate on the Bernoulli Principle and have been described elsewhere [5].

Fig. 2 is a schematic diagram of the top part of the crucible and Mo growth orifice (die) showing a sapphire filament being withdrawn from a thin liquid meniscus pool at the top of the growth orifice. This pool is continuously fed by capillary action from the melt held in the Mo crucible. The o.d. and i.d. of the orifice are 0.027 and 0.013 cm, respectively. Between the orifice and the belt puller (see fig. 1) is located a small-necked down glass pipe containing a liquid, either paraffin, starch, or epoxy, and through which the filament passes. This liquid "bearing" has several functions including that of a coating device and as a sealant protecting the furnace atmosphere from outside contamination. However, its most important function with regard to the present study, is to dampen filament motion occurring as a result of thermal convective currents within the furnace.

2.2. Experimental Procedures

The experimental procedure involved the growth of nominally 0.025 cm diameter *c*-axis Al_2O_3 filament. To avoid minor orientation changes, a single length of filament was grown, during which growth rate and melt temperature changes were made. The main elements of the growth procedure were as follows.

(i) After bringing the crucible etc. to growth temperature, a *c*-axis filamentary seed was lowered into contact with the orifice and, after mutually interacting adjustments of growth rate and melt temperature, growth was established. Growth conditions were adjusted such that "standard" filament was obtained, i.e. filament was grown under melt temperature conditions such that the filament diameter was almost the same as the outside diameter of the orifice. This is basically a trial and error procedure and is easily accomplished with experience.

(ii) The orifice tip temperature was measured using a micro-optical pyrometer operating at a working distance of 12 to 14 cm. These measurements were made through one of the windowless ports.

(iii) A stereo microscope was used to observe the growth area through the other port. Still photographs were taken through one of the eyepieces of the stereo microscope.

(iv) An increase in melt temperature was produced by increasing the power input to the rf coil. A few minutes were allowed for thermal equilibrium to be reached and then steps (ii) and (iii) were repeated.

Temperature increases were not so extreme that the filament would pull free through excessive necking down; thus, after temperature adjustment to allow for the associated change in heat of solidification per minute, a new growth rate was selected and steps (ii), (iii) and (iv) repeated.

Motion picture photography sequences of filament grown under similar changing conditions of growth rate and temperature, as described above, were recorded using a single lens reflex 16 mm camera. Preliminary visual observation had indicated that under certain growth conditions the meniscus region was subject to considerable turbulence; therefore, most of the motion photography was taken at 64

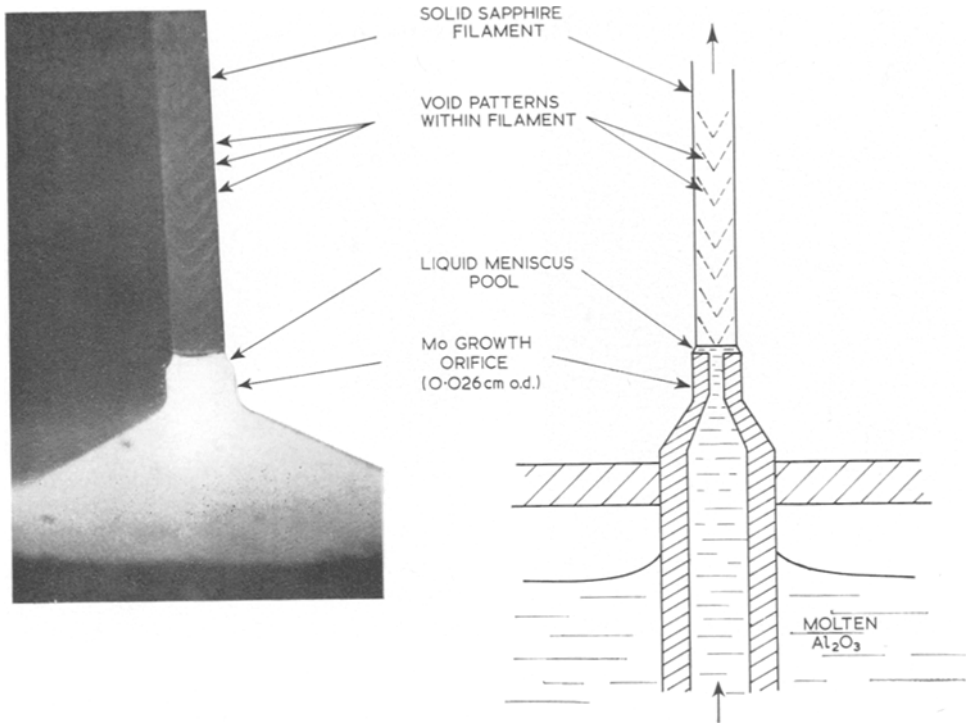

Figure 2 Schematic diagram and corresponding still photograph showing molybdenum growth orifice and sapphire filament being withdrawn from molten meniscus pool.

frames/sec, allowing a clearer visual description of the growth process when the film was projected at normal speed (18 frames/sec) or slower.

Samples of the filamentary sapphire grown under various conditions of temperature and growth speed were examined using transmission optical microscopy. The area to be studied was immersed in oil of refractive index close to sapphire to reduce reflection and refraction at the sapphire/air interface. Sapphire is slightly anisotropic ($n_E = 1.760$ and $n_O = 1.768$) and an oil with $n = 1.760$ was used. The $\langle 0001 \rangle$ growth axis orientation of the filament was confirmed to be within 1° using the Laue X-ray diffraction technique.

3. Results

3.1. Still and Motion Photography Recording Filament Growth

Still photographs and corresponding temperature readings at the orifice tip were obtained for filament grown at rates in the range 3.3 to 7.5 cm/min. Representative series of photographs of the filament growing at the slowest and fastest growth speeds with increasing melt temperatures are presented in figs. 3a, b, c and d and figs. 4a, b and c, respectively. Selected photographs depicting growth at intermediate rates are shown in figs. 5a, b, c and d. These photographs show that the patterns observed in the solid sapphire above the liquid meniscus change dramatically when the growth rate reaches 7.5 cm/min.

The patterns recorded in the solidified sapphire are the result of optical light scattering (within the filament) from microvoids approximately 1 μm in diameter. (Confirmation of the presence of voids within the sapphire may be obtained by examination of the transmission photomicrographs presented in section 3.2.) The most striking observation is the variation in the overall shape of the void layers which occurs for increasing temperature at fixed growth rates of less than 7.5 cm/min. The main characteristic observed in filament grown at 7.5 cm/min is the presence of linear arrays above the orifice tip and within the filament. At slower growth rates, close

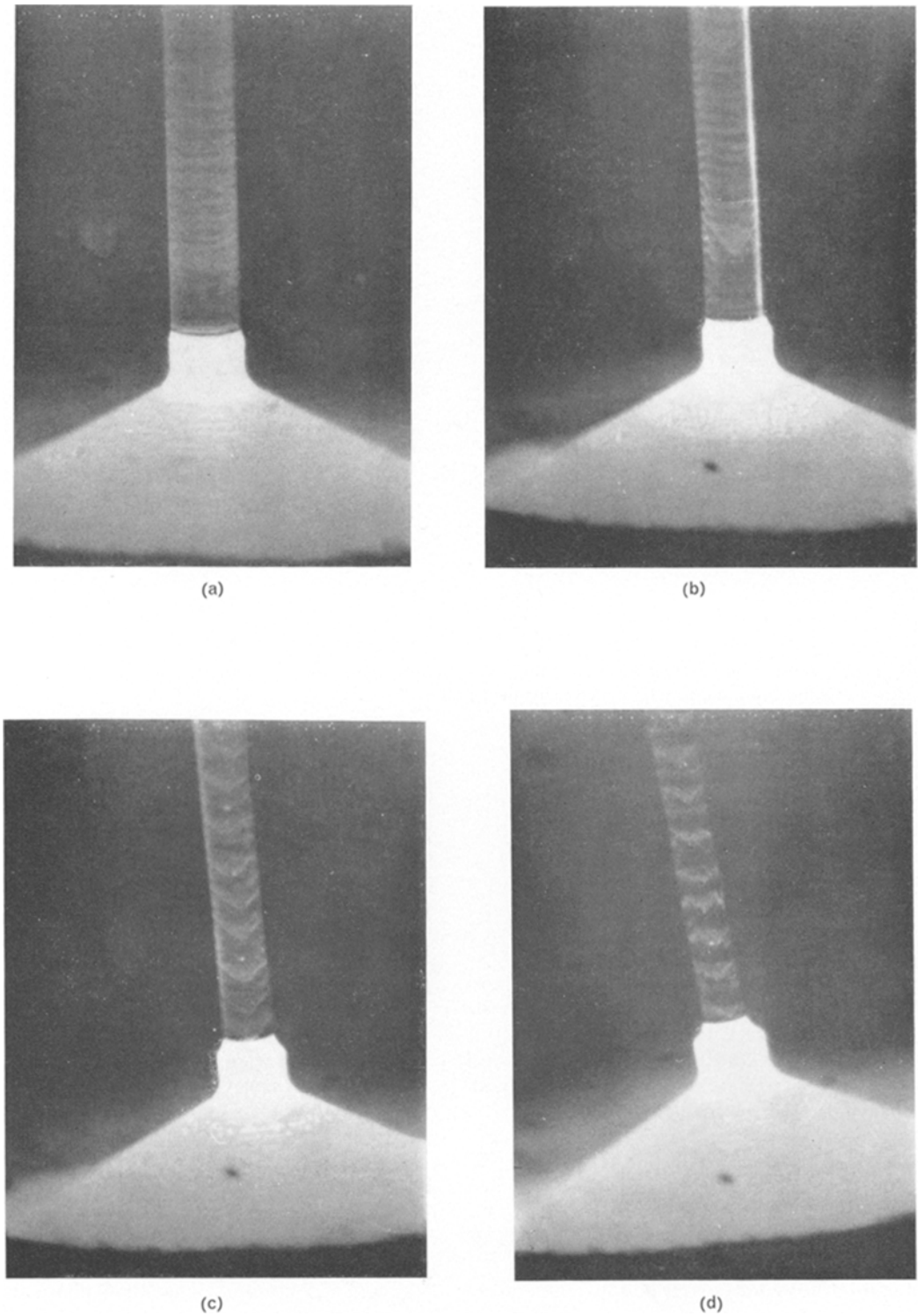

Figure 3 Photographs recording sapphire filament growth at a constant rate of 3.3 cm/min and increasing melt temperature [orifice tip (melt) temperature: a. 2070°C; b. 2090°C; c. 2100°C; d. 2135°C].

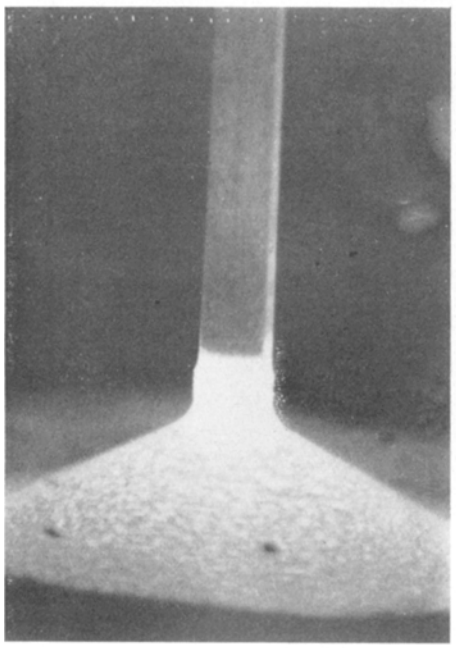

(a)

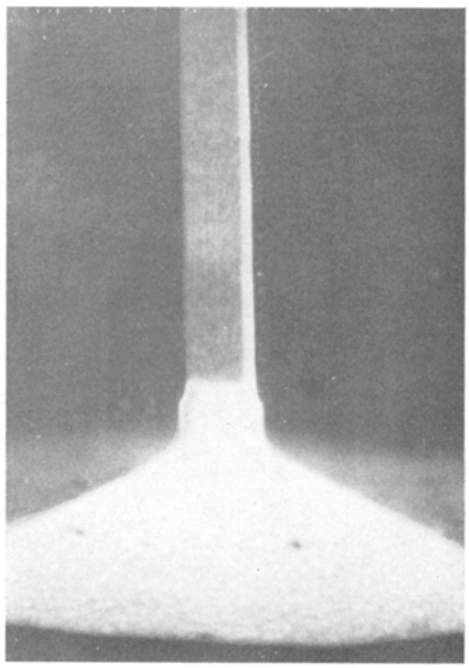

(b)

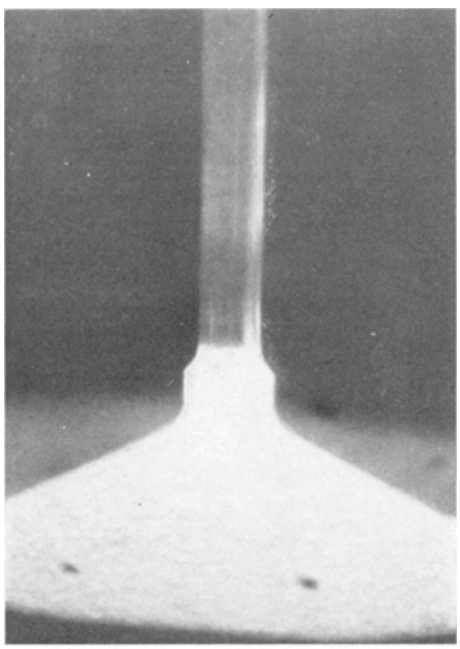

(c)

Figure 4 Photographs recording sapphire filament growth at a constant rate of 7.5 cm/min and increasing melt temperature [orifice tip (melt) temperature: a. 2020°C; b. 2060°C; c. 2100°C].

examination of the void distribution indicates that the void layers deviate from the planarity associated with standard* growth (e.g., figs. 3a and 5b) with increasing temperature, and assume a distinct vee-shaped pattern (e.g., figs. 3b and 5a). The onset of this triangular pattern, with respect to increasing temperature, appears to be related to the growth speed and is associated with a smaller increase in temperature from standard with increasing growth rate. Breakdown of the simple triangular pattern occurs when the growth temperature, as controlled by the rf power setting, deviates an even larger amount from standard (e.g., fig. 3d). At this point the meniscus film height is greater than 0.005 cm and necking down of the filament diameter is severe. The pattern then assumes a dual, triple, or more complicated triangular form. Much larger defects (compared with the microvoids) are evident in several photographs near the centre of the filament (e.g., figs. 3c and d).

The meniscus pool on top of the orifice can vary in thickness between $\sim$ 0.0006 cm (see fig. 3a) and $\sim$ 0.0075 cm (see fig. 5a), depending on the growth speed and temperature. Filament growth from a meniscus whose thickness is out-

*Standard filament growth is defined as filament grown at a melt temperature such that virtually complete outside edge definition by the orifice is obtained.

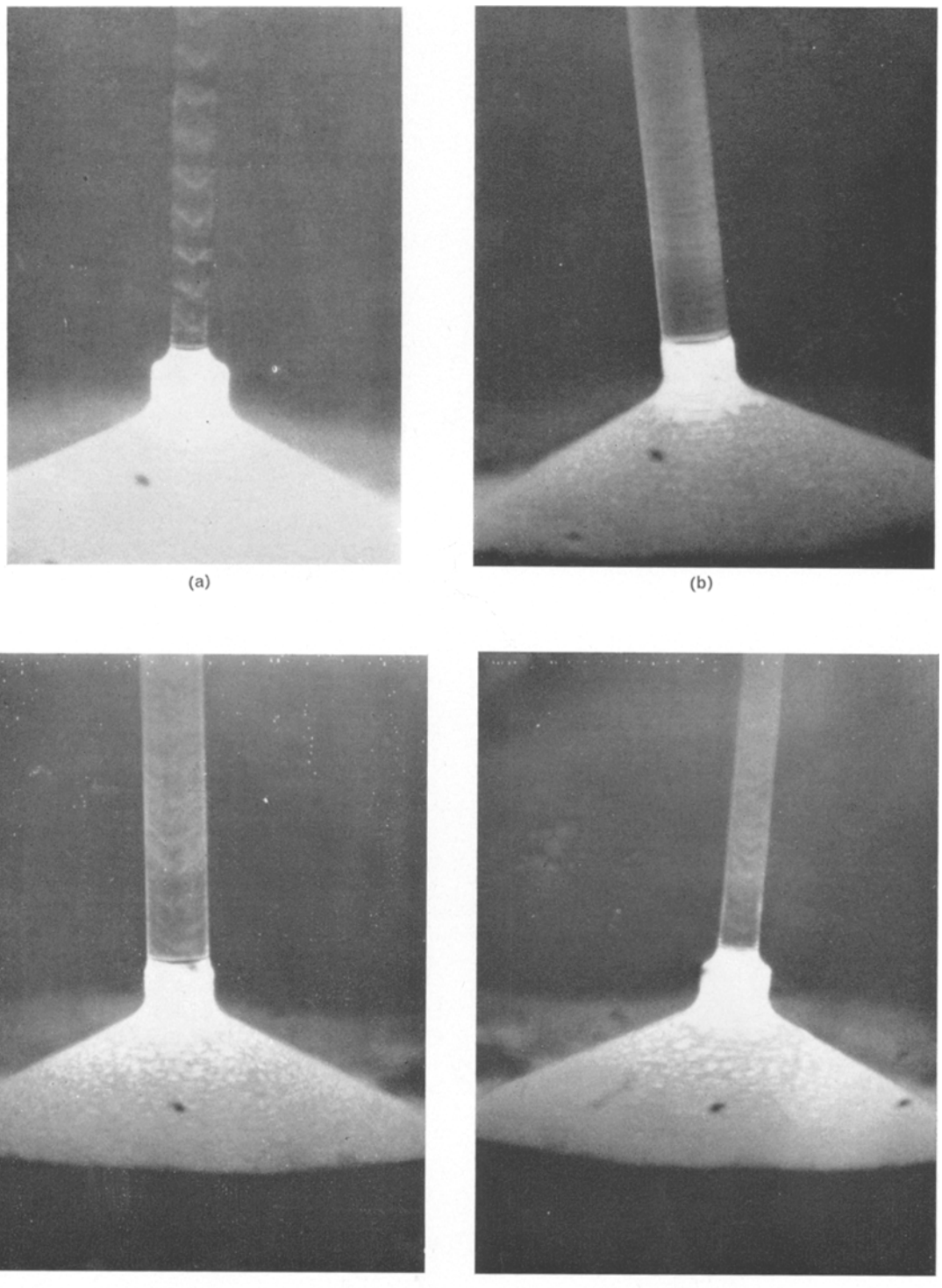

Figure 5 Photographs recording sapphire filament growth in the range 3.8 to 6.0 cm/min (growth rate and melt temperature: a. 4.4 cm/min and 2130°C; b. 5.0 cm/min and 2040°C; c. 6.0 cm/min and 2050°C; d. 6.0 cm/min and 2080°C).

side these limits is not stable. At the lower limit, the filament tends to solidify onto the orifice or to pull free. At the upper limit, necking down of the filament diameter is severe and the filament tends to pull free from the meniscus pool.

Optical temperature readings were not corrected for emissivity variations from unity. The readings were made using the orifice tip which was covered with a thin layer of molten Al_2O_3, and radiated intensely when compared with the surrounding molybdenum surfaces. Molybdenum is reported to have an emissivity of ~ 0.4 at 2000°C [6] and we have assumed the emissivity of molten Al_2O_3 to be close to unity. The growth temperatures recorded over the growth rates investigated are in the range 2020 to 2140°C, compared with the reported melting point for α-Al_2O_3 of 2057 ± 5°C [7]. Comparison between temperatures measured at the orifice tip for different growth conditions is reasonably good, although individual measurements may be in error due wrongly to attributing unity to the emissivity. In general, the variation in growth temperature with growth rate changes is qualitatively consistent with the changing heat of solidification per minute. For example, the temperature measured at the orifice tip for 0.025 cm diameter filament grown at 7.5 cm/min was 2020°C compared with 2070°C for growth of similar diameter filament at 3.3 cm/min.

Filament growth in the range 2.5 to 7.5 cm/min was recorded continuously using 16 mm film [8]. A representative sequence of nine frames, taken when the filament was growing at 3.8 cm/min, is presented in fig. 6. Note that the contrast is reversed. In general, details of structure and growth identical with those reported in the still photographs are observed. The motion photography is poorly used when presented in this fashion, but has proved invaluable in providing visual details of disturbances at the solid/liquid interface when projected at 1 to 10 frames/sec. As a result of the semi-high-speed nature of the photography (64 frames/sec), turbulence within the liquid meniscus during growth at fast rates is particularly apparent. This turbulence is reflected in the microvoids which act as markers. Close examination of the sequence shown in fig. 6 gives some idea of the manner in which this disturbance/void relationship occurs. The appearance of the void layer, immediately above the meniscus, is preceded by a radial movement across the liquid/solid interface towards the centre of the filament. (This may be more obvious if the frames are studied in reverse order.) This disturbance related, void layer production mechanism is an important observation and lends substantial support to the hypothesis that the voids serve to mark the position or relative position of the liquid/solid interface during growth.

3.2. Transmission Photomicrographs

The mid-plane longitudinal cross-sections of filamentary samples were photographed at 0, 45, 90 and 135° intervals of rotation. Figs. 7a, b, c and d, 8a, b, c and d, and 9a, b, c and d present photomicrographs for filament growth at 3.8, 5.0 and 7.5 cm/min, respectively. Microvoids are present in the filament at all growth speeds. In general, these are ~ 1 μm in diameter, although as is evident in fig. 10, they can be much larger. The larger voids which were observed in the still photographs (see figs. 3c and d) are generally found at the apex of the void pattern and can have a similarly oriented distinctive triangular shape. At all growth speeds the filament has an outer shell approximately 0.0025 cm thick, which is entirely free of voids.

The microvoids are observed to lie in patterns which vary with the growth rate and temperature at which the filament was grown. These patterns confirm the aforementioned observation that growth at 7.5 cm/min is radically different from that at slower speeds. At 7.5 cm/min the voids assume essentially linear arrays with respect to the growth axis, although there is some evidence of a spiralling off-axis pattern (see fig. 9). At slower speeds they assume conical dispersions, triangular sections of which were noted in the growth sequence photographs. As shown in fig. 8, a dual pattern is obtained at intermediate growth speeds and/or higher growth temperatures. At slow growth speeds and low orifice tip temperature, the voids in the still photographs taken during growth appear to be in essentially linear arrays with respect to the filament diameter (figs. 3a and 5b). Examination of this filament in transmitted light shows that, in the growth speed range investigated, the overall void dispersion patterns are always conical.

Polished petrographic samples, about 75 μm in thickness, were examined along the growth axis using transmitted light (figs. 11a, b, and c). At growth rates of 6.0 cm/min or less the voids are in distribution patterns which can be recognised as cross-sections of the conical dispersions evident in figs. 7 and 8. However, it is

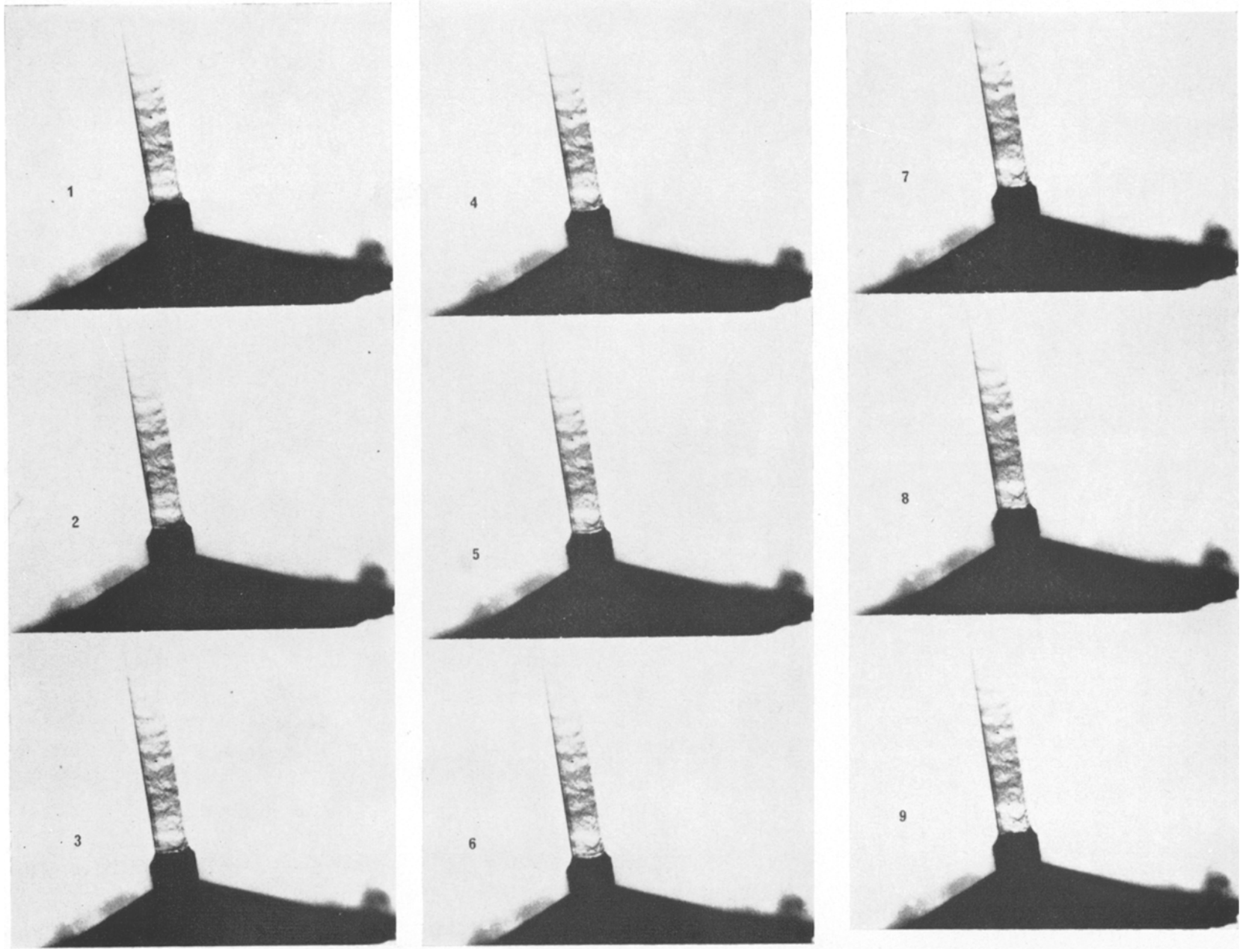
1
2
3
4
5
6
7
8
9

Figure 6 Nine-frame motion photography sequence of growth at 3.8 cm/min. (Contrast is reversed; frame interval 1/64 sec.)

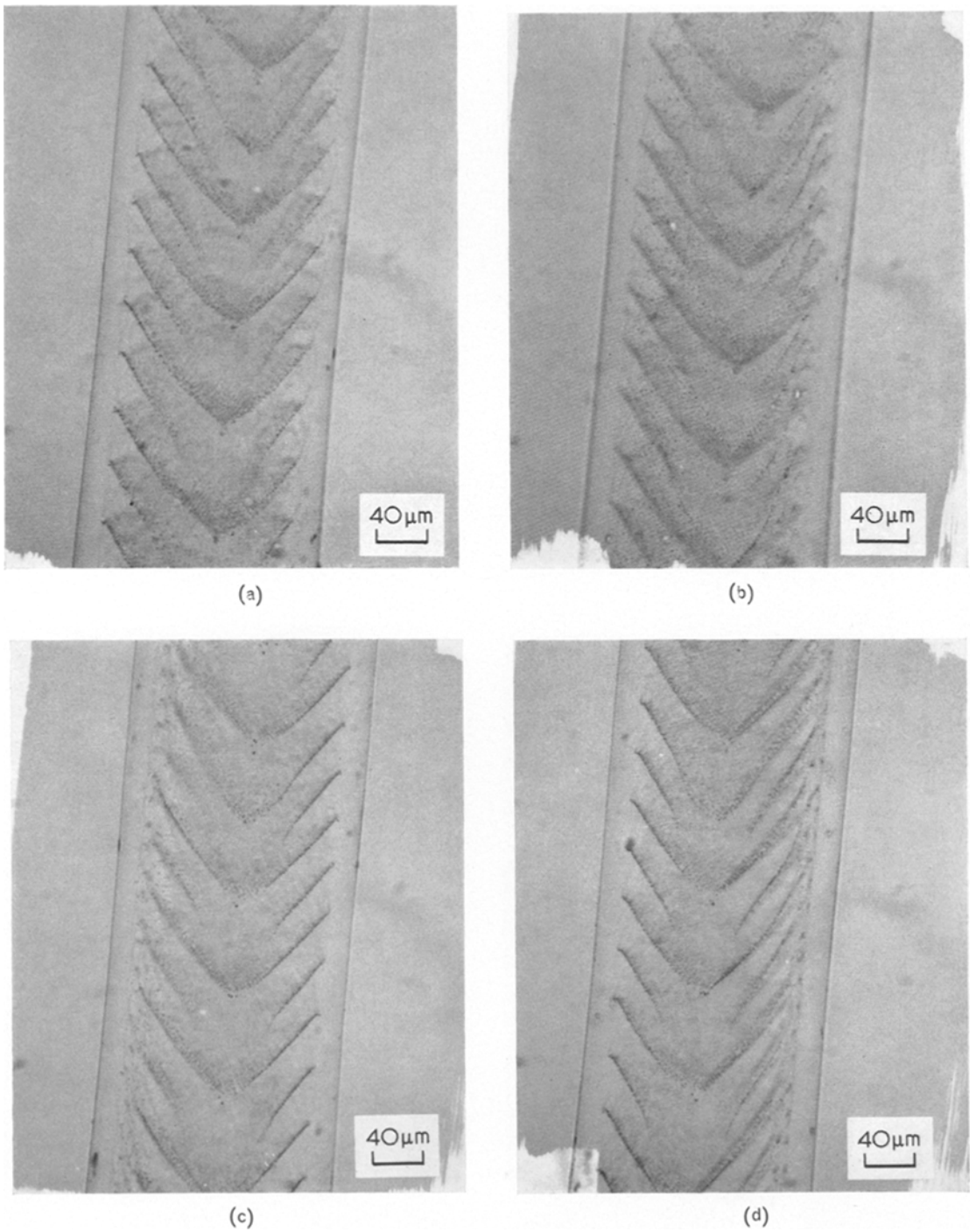

Figure 7 Longitudinal transmission photomicrographs of sapphire filament grown at 3.8 cm/min (degrees of rotation about growth axis: a. 0°; b. 45°; c. 90°; d. 135°).

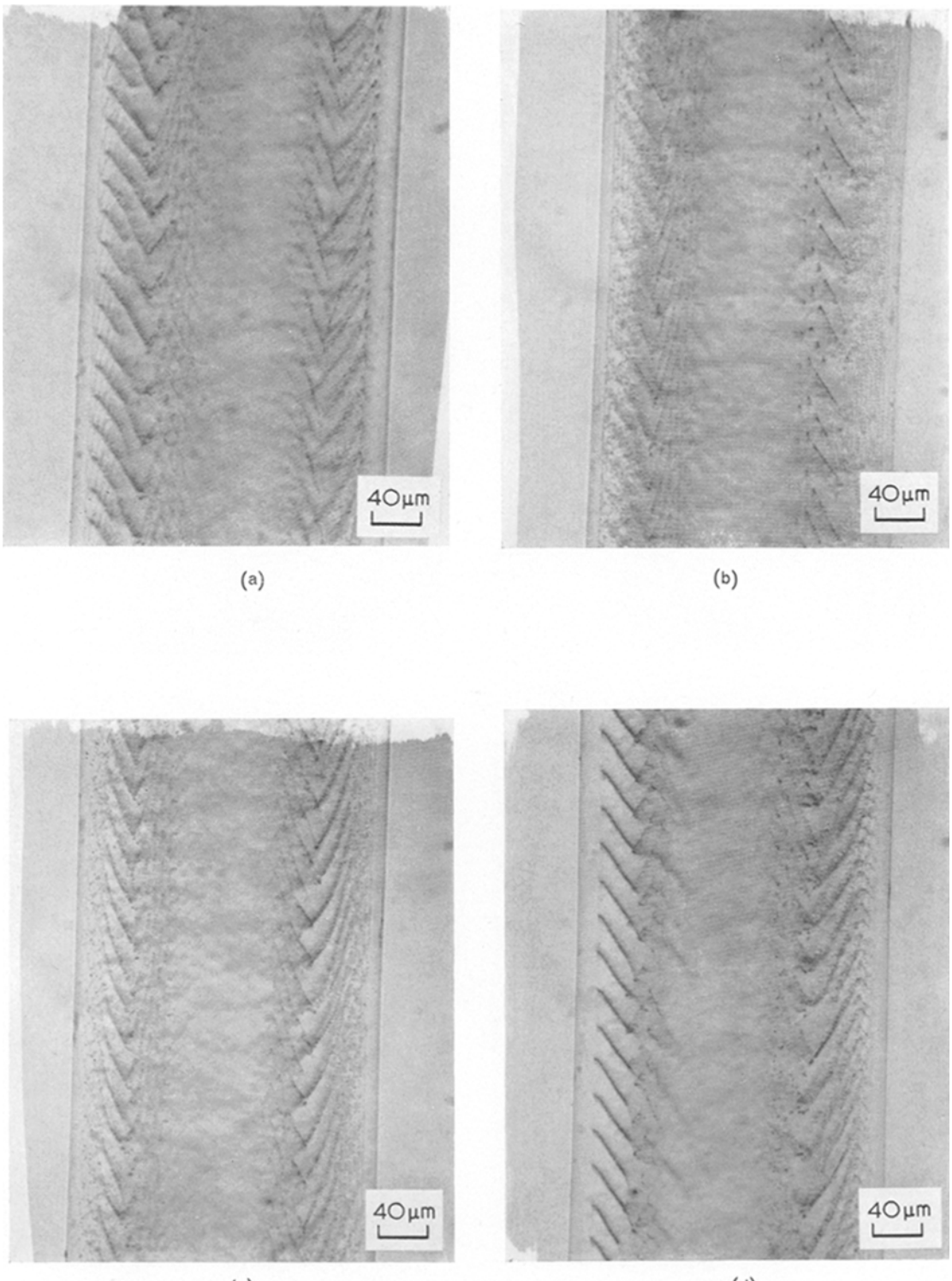

Figure 8 Longitudinal transmission photomicrographs of sapphire filament grown at 5.0 cm/min (degrees of rotation about growth axis: a. 0°; b. 45°; c. 90°; d. 135°).

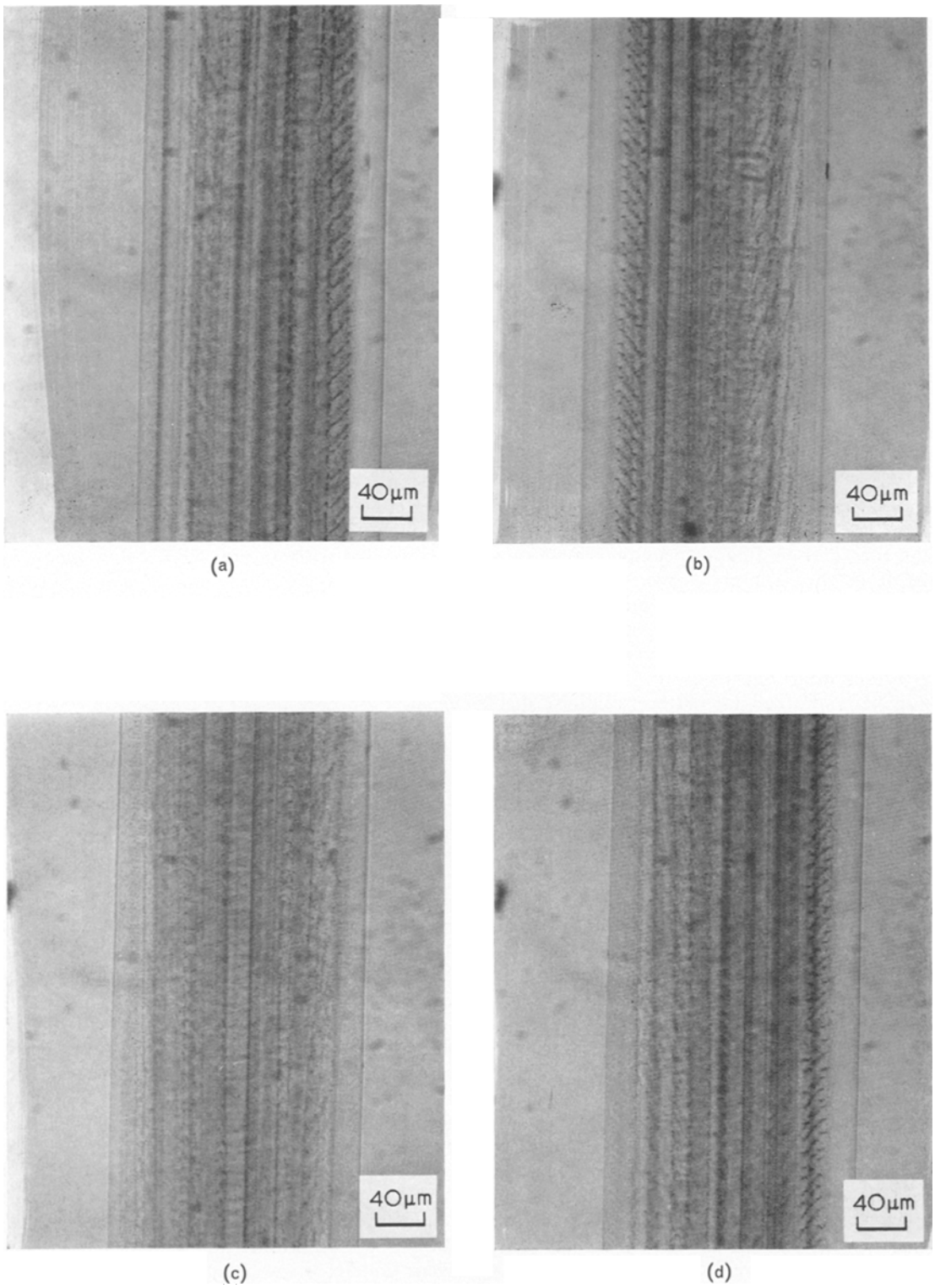

Figure 9 Longitudinal transmission photomicrographs of sapphire filament grown at 7.5 cm/min (degrees of rotation about growth axis: a. 0°; b. 45°; c. 90°; d. 135°).

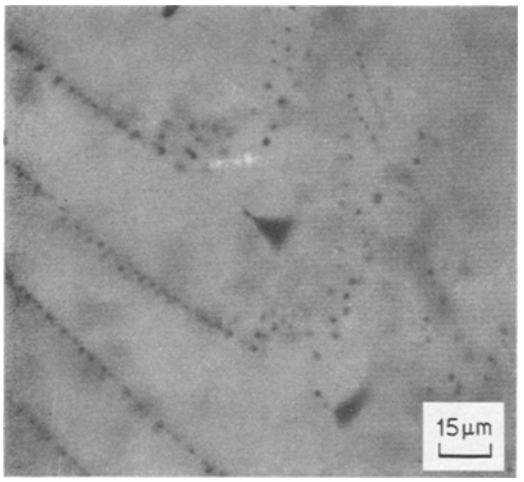

Figure 10 Longitudinal transmission photomicrograph of sapphire filament containing large voids which occupy the apex of the triangular microvoid pattern.

clear that a three-fold dispersion symmetry is present in the sapphire grown at the slowest speeds (fig. 11a). At 6.0 cm/min this conical pattern has begun to break down and a cellular void distribution becomes apparent (fig. 11b). At 7.5 cm/min (fig. 11c) this breakdown is complete, and a cellular pattern, reminiscent of the early work in Pb-Sn alloys by Rutter and Chalmers [9], is present.

4. Discussion

4.1. Filament Micromorphology and the Origin of Microvoids

The microvoid arrays are the most striking characteristic of the sapphire filament growth during the present study. Liquid sapphire has a density of almost 3 g/cc, significantly less than that of 4 g/cc for solid sapphire. Therefore, any growth mechanism or characteristic which allows the entrapment of liquid behind the advancing solid interface would explain void formation. The possible role of gas evolution in directly producing the microvoids is considered subsidiary because of the large number of microvoids and consideration of reported studies on the occurrence of voids in high melting point oxides [10-12]. However, the small segregation coefficient of any gases present would eventually cause their incorporation within the microvoids. Thus, gaseous impurities will be treated as part of the general solute level in the liquid sapphire, and mechanisms for the entrapment of liquid behind the interface will be presented. The mechanisms for void formation and distribution at growth rates greater than 6.0 cm/min will be considered first, followed by presentation of mechanisms at rates in the range $\sim$ 2.5 to 6.0 cm/min.

4.1.1. Growth at rates greater than 6.0 cm/min

In an earlier paper [4] the dendritic nature of growth at very fast growth rates, approximately 16 cm/min, was clearly indicated in scanning electron micrographs of growth interfaces obtained by rapidly removing the crystal from the melt. It was demonstrated that the advancing dendrites in $\langle 0001 \rangle$ growth axis sapphire were capped by well formed $\{10\bar{1}2\}$ rhombohedra, whose trigonal apices pointed in the growth direction. The occurrence, or tendency towards the necessary thermal supercooled liquid conditions for dendritic growth was confirmed during the present work. With increasing rate of growth, the melt temperature had to be continuously lowered and temperatures 40° C below the melting point of sapphire were measured at the orifice for the fastest growth rates. When dendritic growth occurs, void origin may be explained as the end result of liquid entrapment between dendrites and dendrite side arms. Extreme examples of the result of this mechanism, observed in sapphire grown at $\sim$ 11 cm/min, are shown in fig. 12. Many of the shrinkage voids are no longer spherical and are distinctly elongated. A description and discussion of dendritic growth using the photographic recording methods of the present study will be reported elsewhere [13].

During the present study it was noted that growth at 7.5 cm/min was markedly different from that at slower speeds, at least in so far as the final void distributions are concerned. Although linear arrays are observed in dendritically grown sapphire filament, in general, the voids assume patterns which are similar in overall appearance to those observed at slower speeds ($<$ 6.0 cm/min), with the aforementioned difference that the voids themselves are no longer necessarily spherical. The linear void arrays displayed in figs. 9a, b, c and d and the corresponding transverse section in fig. 11c for filament grown at 7.5 cm/min, are strongly suggestive of cellular growth caused by constitutional supercooling, the occurrence and theory of which has been widely investigated since it was first reported in 1953 by Rutter and Chalmers [9]. The microvoids occupy cell defining positions

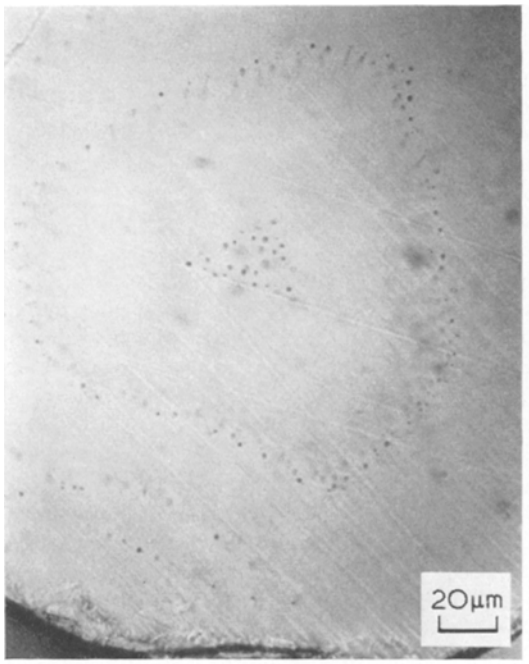

(a)

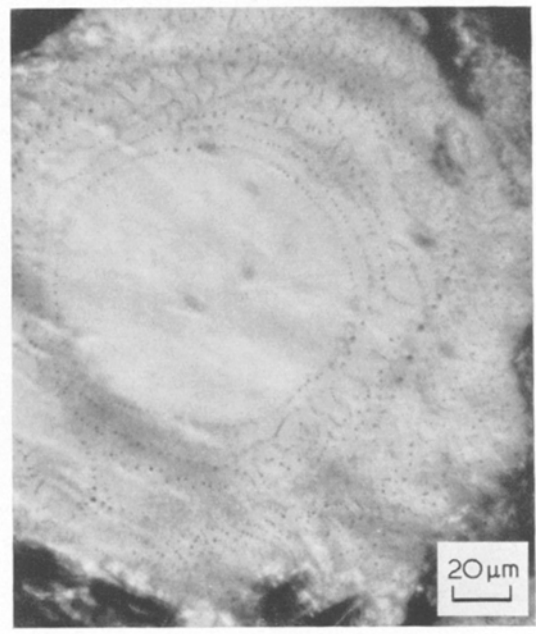

(b)

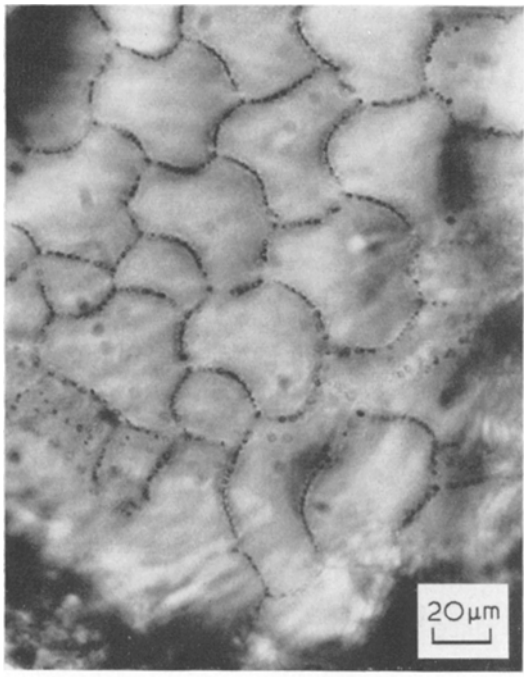

(c)

Figure 11 Transverse transmission photomicrographs showing the microvoid distribution on the sapphire filament growth plane (0001) (growth rate: a. 3.3 cm/min; b. 6.0 cm/min; c. 7.5 cm/min).

corresponding to the lower melting point, solute-rich areas observed when constitutional supercooling occurs during the directional solidification of binary metal systems such as Pb-Sn and Pb-Sb.

Since thermally controlled dendritic growth has been observed at slightly higher growth rates

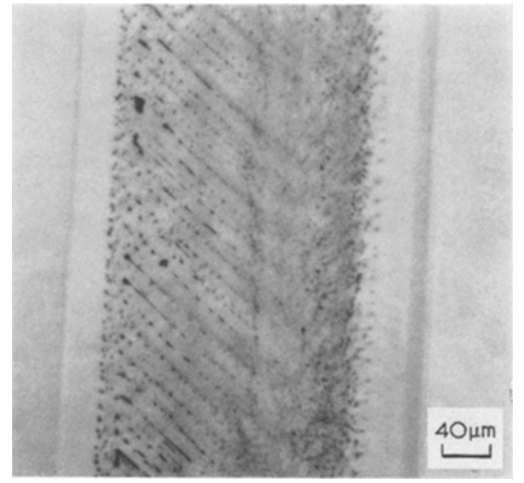

Figure 12 Longitudinal transmission photomicrograph of sapphire filament grown dendritically at ~ 12 cm/min.

($\sim$ 10 cm/min) [13], it is probable that the cellular growth observed at 7.5 cm/min is a preceding stage and the result of less extreme thermal supercooling of the melt in front of the advancing solid interface. However, the possible role of constitutional supercooling must be considered, particularly when the very fast non-dendritic growth rates achieved by EFG are taken into account.

The condition for the occurrence of constitutional supercooling is given by [14]

$$\frac{G}{V} \leq -\frac{mC_s(1-k_0)}{k_0 D_L}$$

where G is the temperature gradient in the liquid at the growth interface, m is the liquidus slope for the impurity considered, C_s is the impurity concentration, k_0 is the effective distribution coefficient, and D_L is the diffusion coefficient for the impurity in the liquid. For typical values, $G = 10°\text{C/cm}$, $m = -3°\text{C/at. \%}$, $C_s = 50$ ppm (Mo + Si + Ti + Mg + Ni + Cr), $k_0 = 0.5$, and $D_L = 10^{-5}$ cm^2/sec, constitutional supercooling would occur for growth rates V greater than about 0.5 cm/min. Clearly, with growth rates in the range 2.5 to 7.5 cm/min during the present study, the possibility of constitutional supercooling may not be ignored. Also, Cockayne *et al* [12] observed that the occurrence of micro-voids in c-axis Czochralski sapphire grown at $\sim$ 0.02 cm/min could be correlated with the presence of impurities in the charge material. Thus, during dendritic and cellular growth of sapphire by EFG the growth mechanism may be controlled by both thermal and constitutional supercooling.

4.1.2. Growth in the range 2.5 to 6.0 cm/min

The void patterns at slower growth rates ($<$ 6.0 cm/min) are dissimilar from the impurity controlled microstructures observed with binary metal alloys in the stage preceding cellular growth [15]. Close examination of the transverse sections of samples grown at 5 and 6 cm/min (fig. 11b) does indicate, however, in agreement with Tiller [15], a tendency towards elongated cells in the off-centre region. The patterns of voids in the growth range 3.3 to 6.0 cm/min (figs. 7 and 8) are distinctively angular and, as mentioned previously, these arrangements are similar to those observed in c-axis material grown by dendritic propagation of $\{10\bar{1}2\}$ rhombohedra. Measurement of the angle made by the void arrays with the c-axis for filament grown at speeds in the range 3.3 to 6.0 cm/min leads to values centred around 56°. These values are close to the angles measured for similarly arranged solidification voids in the dendritically grown material (see fig. 12), and are in agreement with angles measured between rhombohedral surface planes and the c-axis using crystal dendrites and two circle optical goniometry [4]. Also, a distinctive three-fold symmetry is noted in micrographs of transverse sections of samples grown at 3.3 cm/min (see fig. 11a). It may be concluded from this relationship between the void distribution and the rhombohedral planes that these rhombohedral planes play a major role in the growth of c-axis sapphire by EFG at 3.3 to 6.0 cm/min.

The following observations are also pertinent and require explanation within a model proposed for void formation and distribution during EFG at speeds up to $\sim$ 6.0 cm/min. A void free outer shell varying in thickness between 0.0006 and 0.0025 cm is noted. Examination of consecutive frames of the 16 mm motion photography has indicated that the void arrays are started near the filament surface and are the result of a mechanism, involving a growth front, which moves towards the centre of the filament as the latter is withdrawn from the top of the orifice. This latter observation is confirmed by the overall void patterns and the presence in several longitudinal transmission micrographs, of large triangular voids occupying the apex of the void arrays (fig. 10).

Crystal growth by the EFG method differs from other techniques in several distinct ways, including the capillary feeding action from the melt to the top of the shaping orifice and the efficient heat loss mechanism from the growth region by means of radiation to the watercooled furnace walls. These characteristics are particularly evident in the present case, in which the rate of liquid flow in the capillary and across the orifice surface will be up to five times the crystal withdrawal rate, and the growth orifice is placed deliberately high with respect to the carbon susceptor and rf coil, so that radiative heat loss to the quartz furnace walls might be as efficient as possible. During cellular growth, the solid/liquid interface, while non-planar, is evidently stable over periods of time such that linear void arrays outlining the cell walls are obtained. Examination of the cell walls at depths of up to 200 μm within the filament indicates that most of the cells retain essentially the same dimensions, only

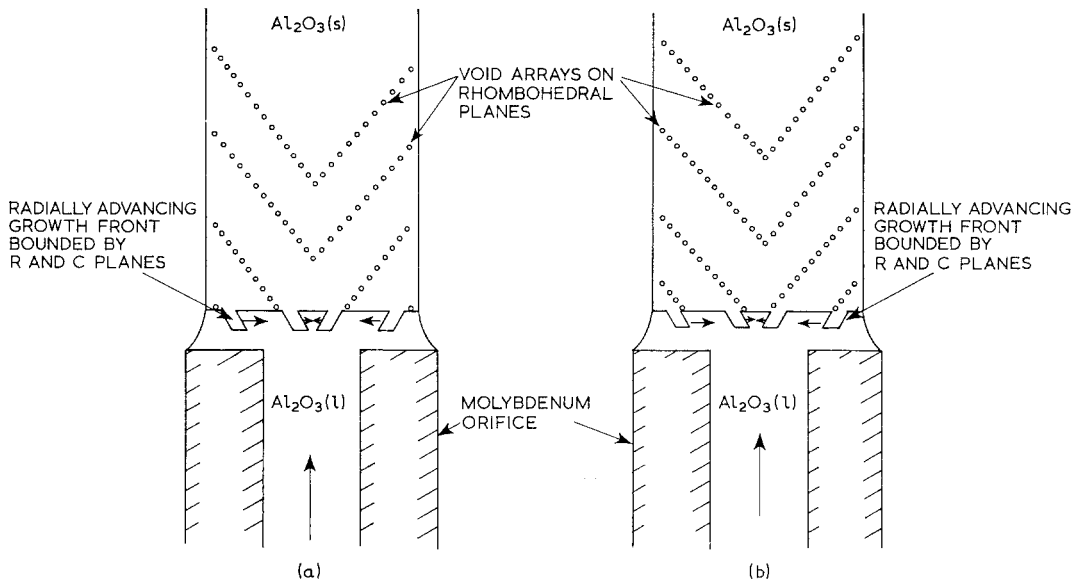

Figure 13 Schematic representations of void formation and distribution mechanisms (a. *Behind* the crystal projection due to turbulence and inadequate liquid supply; b. *In front of* the crystal projection due to constitutional supercooling).

a few cells growing out or being created. This is not true for growth at slower rates, where the transmission photomicrographs and motion photography show that solidification occurs first above the outer edge of the orifice forming a void-free shell. Therefore, the effect of radiative heat loss from the meniscus surface is significant at slower growth rates. The radially advancing interface may then be considered as a projection resulting from the intersection of rhombohedral planes and consecutive *c*-planes (see fig. 13). Growth towards the orifice will be inhibited by the top surface and increasing melt temperature. Thus, liquid supply from the capillary to the outside of the orifice may be restricted due to the narrow passage present between the interface projection and the top surface of the orifice. Turbulence, as a result of this constriction, may also be expected, and the overall result could be a limited liquid supply to the step intersections between the rhombohedral and *c*-planes, and the formation of voids *behind* the advancing interface as a result of a pinching off mechanism. This void formation mechanism is shown schematically in fig. 13a. Another mechanism based on constitutional supercooling is also possible. Consider a similarly shaped growth interface and the effect of radiative heat loss such that the outside of the meniscus will be the coolest part of the growth interface. The melt could become supersaturated with respect to impurity atoms as solidification proceeded. Impurity rejection on solidification could result in constitutional supercooling *in front of* the radially advancing interface, and voids would be formed by a pinching off mechanism and retention of lower melting point liquid. This is presented schematically in fig. 13b and is essentially a cellular mechanism modified by the presence of a radial temperature gradient. As discussed in section 4.1.1, because of the substantial growth rate achieved with EFG, this impurity controlled constitutional hypothesis may not be discounted.

In both of these void formation and distribution mechanisms, the periodicity of the void layers with respect to the growth axis is a consequence of the need to supercool (or supersaturate) the liquid at the edge of the orifice before solidification can begin. When the growth front interface forms, the liquid temperature is raised due to the heat of solidification released (or the impurity atoms are consumed). Thus, the growth front moves radially towards the centre of the growth zone, leaving behind liquid sapphire which has to be further cooled (or supersaturated) before solidification can occur again at that part of the solid/liquid interface.

In summary, during cellular growth at 7.5

cm/min a stable interface, essentially unmodified by radiative heat loss from the outside of the meniscus film, is present. The conditions for this growth mode are created either by thermal supercooling of the liquid in front of the growth interface, as a result of lowering of the bulk melt temperature (an experimentally observed fact), or as a result of impurity rejection on solidification and the creation of conditions under which constitutional supercooling can occur. In the growth rate range 2.5 to 6.0 cm/min the role of radiative heat loss and the resultant radial thermal gradient becomes important. Void formation mechanisms, either pinching off due to insufficient liquid flow to growth interface step intersections or constitutional supercooling due to impurity rejection at similarly stepped interfaces, are effected by the radial thermal gradient, and crystallographically controlled, conical void arrays are obtained. Recently, *c*-axis sapphire filament entirely free from the microvoids discussed here has been grown at speeds up to 2.5 cm/min. This work is continuing and details will be presented when the study is complete [16]. However, it is already apparent, in agreement with the present study, that the major controlling parameter is the temperature profile at the growth interface and that the attainment of a significant positive thermal gradient from the melt to the solid is of primary importance.

4.2. Factors Effecting Filament Diameter and Growth Stability

Chalmers, LaBelle, and Mlavsky [3] have discussed the conditions for stable growth under ideal conditions where perturbations due to liquid turbulence and lateral physical movement of the filament are not considered. Provided the basic criteria for EFG are satisfied, i.e. capillary rise and fulfilment of contact angle requirements within the meniscus film, stable growth will occur when there is a continuous balance between the various thermal processes occurring within the meniscus. For stable growth at rate V, the sum of heat arriving at the solid/liquid interface H_L and heat generated there H_S (heat of solidification), must equal heat losses via radiation and conduction into the solid sapphire H_C and from the meniscus surface H_M. This thermal balance may be expressed in the relationship:

$$V \cdot H_S + H_L = H_C + H_M ,$$

where H_L may be positive or negative depending on the sign of the thermal gradient in front of the growing interface. Qualitatively, the thermal balance expressed in this equation is confirmed by the observations made during the present study. For example, melt temperature increases made at constant growth speed (i.e. positive additions to H_L) cause a reduction in filament diameter (H_C and H_S decreasing) and an increase in the thickness of the liquid meniscus from which the filament is withdrawn (H_M increasing). Table I presents data describing this relationship for filament grown at 4.4 cm/min.

TABLE I Growth temperature, filament diameter and effective meniscus area for growth at 4.4 cm/min (melt temperature increasing).

Temperature measured at orifice tip (°C)	Filament diameter (cm)	Meniscus height (cm)	Meniscus surface area (cm^2)
2040	2.4×10^{-2}	1.6×10^{-3}	1.8×10^{-4}
2070	2.3×10^{-2}	3.8×10^{-3}	3.3×10^{-4}
2090	2.2×10^{-2}	4.3×10^{-3}	3.7×10^{-4}
2105	2.0×10^{-2}	5.2×10^{-3}	4.6×10^{-4}
2120	1.7×10^{-2}	6.4×10^{-3}	5.5×10^{-4}
2145	1.3×10^{-2}	7.1×10^{-3}	6.2×10^{-4}

These data were obtained by enlarging still photographs (e.g. figs. 3 to 5) and are typical for growth in the range 3.3 to 6.0 cm/min, where it is found that the filament diameter/meniscus height ratio for a given filament diameter is nearly constant. Filament diameter is shown plotted versus meniscus height for the data in fig. 14, and it is clear that with increasing meniscus height the filament diameter becomes increasingly

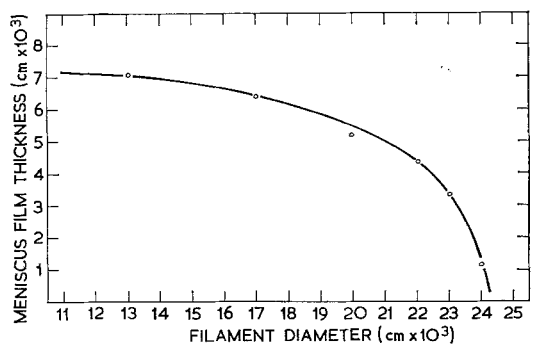

Figure 14 Filament diameter versus meniscus film thickness for growth at 4.4 cm/min.

unstable with respect to additional small changes in meniscus height. In other words, the filament diameter becomes progressively less stable to melt temperature fluctuations as its size deviates from that of the orifice outside diameter.

The stability of the filament diameter as a function of temperature fluctuations at different growth speeds has also been considered. Using temperatures measured at the orifice and the corresponding filament diameter, the ratio, decrease in filament diameter to increase in temperature, has been calculated for each growth speed. These data are plotted in fig. 15, indicating that for increasing growth rates up to 6.0 cm/min the filament diameter becomes increasingly unstable with respect to changes in temperature. The data point for growth at 7.5 cm/min has not been included since growth at this speed is unstable, and filament of varying diameter may be grown under conditions of constant growth rate and temperature. Indeed, as the growth rate is further increased the crystal shape is no longer defined completely by the orifice diameter, even for small meniscus heights, and assumes a distinctly rounded triangular cross section [4].

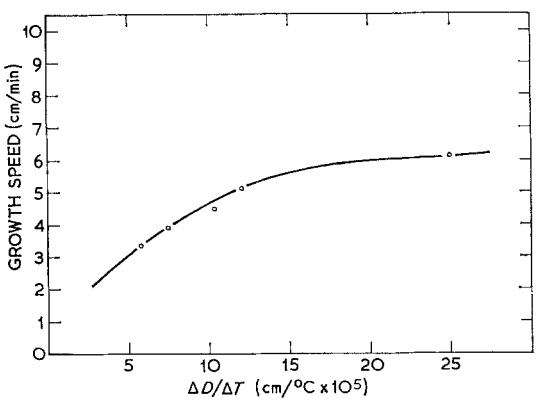

Figure 15 Growth speed versus the ratio of the change in filament diameter ΔD to associated increase in melt temperature Δdt.

5. Summary and Conclusions

An experimental study of the continuous melt growth of *c*-axis sapphire filament has been presented. This filament had a nominal 0.025 cm diameter and was grown in the range 2.5 to 7.5 cm/min using the edge-defined, film-fed growth (EFG) technique. Filament growth was recorded using both still and 16 mm motion photography, and samples grown have been subjected to examination using transmitted light metallographic and petrographic methods.

During growth, the following are the major observations:

(i) Patterns of 1 μm voids are observed at all growth speeds, the shape of these patterns being a function of temperature and growth rate.

(ii) At 6.0 cm/min or slower growth rates, the void patterns are conical. The apices of these cones point towards the melt and may be occupied by a single, substantially larger void ($\sim$ 10 μm). A single cone is generally observed at low growth temperatures, a dual or triple puckered form being associated with increasing growth temperature and increasing meniscus film thickness.

(iii) At 7.5 cm/min, the main visual characteristics are linear void patterns observed to lie parallel to the filament longitudinal axis.

(iv) The 16 mm motion photography recorded at 64 frames/sec, confirms these points and when projected in single frame sequence suggests that at growth speeds < 6.0 cm/min, the voids are produced as the result of a radially moving growth front at the liquid/solid interface.

Transmission photomicrography validates these growth observations, and shows that at 7.5 cm/min, the voids occur in dispersions outlining the edges of substructural cells which extend along the filament longitudinal axis, whereas at slower speeds they lie essentially on cones, triangular sections of which were photographically recorded during growth. At the slowest growth speeds a distinctive three-fold dispersion symmetry is evident in transverse sections.

It is suggested that the cellular growth observed at 7.5 cm/min is the result of thermal supercooling. However, at the fast growth rates achieved with EFG the possibility of a contributing role from impurity dependent constitutional supercooling may not be entirely ruled out. The void origin under conditions of cellular growth is therefore the result of liquid entrapment at the interface cell walls which, due to the large difference in density between liquid and solid sapphire, results in the formation of voids after solidification.

In material grown more slowly, measurement of the angles made by the void dispersions with the filament axis indicates that these voids lie in or near the sapphire rhombohedral $\{10\bar{1}2\}$ planes. It is suggested that in the growth range

up to 6.0 cm/min, solidification is controlled by a radial thermal gradient and starts first from above the orifice outer edge. Solidification then continues radially inwards by means of a moving crystalline projection bounded by the rhombohedral and basal planes. Voids are formed under these circumstances either as a result of insufficient liquid supply *behind* the moving projection interface, or solute rejection and constitutional supercooling *in front of* the interface.

Qualitatively, growth stability in the EFG system is found to be dependent on a thermal balance between the various thermal generation and transfer mechanisms occurring within the meniscus. Data of the growing crystals and corresponding temperature measurements show that at constant growth rate the filament diameter becomes increasingly unstable with respect to increases in melt temperature. Also, the filament diameter becomes less stable with respect to melt temperature fluctuations as the growth rate increases.

Acknowledgements

The author wishes to thank J. Bailey for his excellent experimental assistance and many helpful technical discussions. He also wishes to acknowledge many stimulating discussions with H. E. LaBelle, Jun and G. F. Hurley.

This work was supported by the US Air Force Materials Laboratory, Nonmetallic Materials Division, Wright-Patterson Air Force Base, Dayton, Ohio.

References

1. H. E. LABELLE, JUN and A. I. MLAVSKY, *Mater. Res. Bull.* **6** (1971) 571.
2. H. E. LABELLE, JUN, *ibid* **6** (1971) 581.
3. B. CHALMERS, H. E. LABELLE, JUN, and A. I. MLAVSKY, *ibid* **6** (1971) 681.
4. H. E. LABELLE, JUN and J. T. A. POLLOCK, *ibid*, to be published.
5. *Idem, Rev. Sci. Instrum.* **42** (1961) 160.
6. "Thermophysical Properties of High Temperature Materials", edited by T. S. Touloukien, **1** McMillan, New York, (1967) 675.
7. National Bureau of Standards Special Publication No. 325, p. 117 (1970).
8. Part of this film was shown at the International Crystal Growth Conference, Marseilles, France, 1971.
9. J. W. RUTTER and B. CHALMERS, *Can. J. Phys.* **31** (1953) 15.
10. W. BARDSLEY and B. COCKAYNE, *Proc. Int. Conf. Cryst. Growth* (Boston 1966), *Suppl. J. Phys. Chem. Solids* (1967) 109.
11. C. A. MAY and J. S. SHAH, *J. Mater. Sci.* **4** (1969) 179.
12. B. COCKAYNE, M. CHESSWAS, and D. B. GASSON, *ibid* **2** (1967) 7.
13. J. T. A. POLLOCK and J. BAILEY, unpublished work.
14. W. A. TILLER, J. W. RUTTER, K. A. JACKSON, and B. CHALMERS, *Acta Metallurgica* **1** (1953) 428.
15. W. A. TILLER, in "The Art and Science of Growing Crystals", edited by J. J. Gillman, (J. Wiley and Sons, New York, 1963) p. 276.
16. J. T. A. POLLOCK, *J Mater. Sci.* accepted for publication.

Received 20 August and accepted 1 October 1971.